Quantifying the contribution of ship noise to the underwater sound field

Najeem Shajahan, David R. Barclay, and Ying-Tsong Lin

Citation: The Journal of the Acoustical Society of America **148**, 3863 (2020); doi: 10.1121/10.0002922
View online: https://doi.org/10.1121/10.0002922
View Table of Contents: https://asa.scitation.org/toc/jas/148/6
Published by the Acoustical Society of America

JASA ARTICLE

Quantifying the contribution of ship noise to the underwater sound field

Najeem Shajahan,[1] David R. Barclay,[1,a)] and Ying-Tsong Lin[2]
[1]*Department of Oceanography, Dalhousie University, 1355 Oxford Street, Halifax, Nova Scotia B3H 4R2, Canada*
[2]*Applied Ocean Physics and Engineering Department, Woods Hole Oceanographic Institution, 266 Woods Hole Road, Woods Hole, Massachusetts 02543-1050, USA*

ABSTRACT:
The ambient sound field in the ocean can be decomposed into a linear combination of two independent fields attributable to wind-generated wave action at the surface and noise radiated by ships. The vertical coherence (the cross-spectrum normalized by the power spectra) and normalized directionality of wind-generated noise in the ocean are stationary in time, do not vary with source strength and spectral characteristics, and depend primarily on the local sound speed and the geoacoustic properties which define the propagation environment. The contribution to the noise coherence due to passing vessels depends on the range between the source and receiver, the propagation environment, and the effective bandwidth of the characteristic source spectrum. Using noise coherence models for both types of the sources, an inversion scheme is developed for the relative and absolute contribution of frequency dependent ship noise to the total sound field. A month-long continuous ambient sound recording collected on a pair of vertically aligned hydrophones near Alvin Canyon at the New England shelf break is decomposed into time-dependent ship noise and wind-driven noise power spectra. The processing technique can be used to quantify the impact of human activity on the sound field above the natural dynamic background noise, or to eliminate ship noise from a passive acoustic monitoring data set. © *2020 Acoustical Society of America*. https://doi.org/10.1121/10.0002922

(Received 11 August 2020; revised 29 October 2020; accepted 24 November 2020; published online 21 December 2020)
[Editor: D. Benjamin Reeder] Pages: 3863–3872

I. INTRODUCTION

The sound of surface distributed sources, such as breaking waves and rainfall, is ubiquitous in the world's oceans, while noise generated by ships is detectable in nearly every ocean basin (Wenz, 1962). The increase in commercial ship traffic is responsible for an increase of low frequency (0.1–1 kHz) noise by about 3 dB/decade since 1960 due to the global economic growth, with a flattening in recent years (McDonald *et al.*, 2006; Chapman and Price, 2011; Frisk, 2012; Miksis-Olds and Nichols, 2016; Harris *et al.*, 2019). Noise produced by vessel traffic dominates the typical deep ocean spectrum below 1 kHz, while above that the sound of wind-generated breaking waves prevails. The resultant ambient noise field at low frequencies depends on ship traffic density and ship source spectrum level, and can be as much as 40 dB higher than the typical wind noise levels in the same band (Wales and Heitmeyer, 2002). Increases in anthropogenic noise due to shipping can mask the effective communication range, alter habitat use, impact behavior, and increase stress among marine species, and are a growing concern for researchers working in marine ecology (Rolland *et al.*, 2012; Popper and Hawkins, 2016; Putland *et al.*, 2018). As a result, Passive acoustic monitoring (PAM) has become widely used in ocean monitoring, and long-term ambient sound recordings have been used with automatic identification system data and sound propagation models to study and map the impact of ship traffic on the marine habitat (Erbe *et al.*, 2012; Merchant *et al.*, 2012; Gervaise *et al.*, 2015; Aulanier *et al.*, 2017). These approaches use metrics derived from power or pressure spectral density to study the marine soundscape and the potential impacts of anthropogenic sound sources on the overall noise field and marine animals. However, because of the dynamic nature of natural ambient noise driven by wind speed and direction, sea-surface roughness, bathymetry, fetch (Vagle *et al.*, 1990), surface current speed and direction, and rainfall (Nystuen *et al.*, 1993), quantifying the contribution of anthropogenic sources above the changing background level is challenging. In this work, a method of source separation based on the linear decomposition of the directionality and vertical coherence into surface-generated, and distant and close-range vessel-generated noise components is used to quantify the time series of the relative and absolute contribution of shipping activity to the undersea soundscape in a month long data set.

In shallow water the spatial properties of the ambient noise generated by surface distributed sources, including the directionality, depend on the bathymetry, water column sound speed, and sediment geoacoustic properties. In the case of the seabed with a sound speed faster than that in the water, the critical angle can be measured and used to estimate the value of the compressional sound speed in the sediment (Buckingham and Jones, 1987). The normalized

a)Electronic mail: dbarclay@dal.ca, ORCID: 0000-0002-3810-1662.

cross-spectral density, or the vertical noise coherence, is directly related to the directionality (Cox, 1973) and can be used to infer the geoacoustic properties in a Pekeris (fluid) wave guide (Deane *et al.*, 1997), a shallow water elastic wave-guide (Carbone *et al.*, 1998), and a multilayered seabed (Barclay *et al.*, 2019). Direct measurements of noise directionality, coherence, and cross-correlation, using beamformed vertical line arrays (VLAs) and model-based matched field processing techniques, have been performed to invert for high-resolution bottom reflection loss coefficients (Siderius *et al.*, 2013; Muzi *et al.*, 2015; Muzi *et al.*, 2016; Muzi *et al.*, 2018), and to passively detect the seafloor depth and sub-bottom layering (Siderius *et al.*, 2006). It has been shown that the water column sound speed profile and attenuation in the deep ocean can be inverted using the vertical coherence of ambient noise (Barclay and Buckingham, 2013a; Buckingham, 2013).

The noise coherence is a normalized quantity, independent of the time-varying frequency-dependent power spectral density (PSD) typically observed in ocean noise. It is insensitive to source strength, and the slope and spectral shape of the background noise which can vary from site to site in shallow water (Ingenito and Wolf, 1989). In inversion applications, the stability and wideband nature of the vertical noise coherence function allow estimates of seabed bottom loss and sub-bottom structure (Siderius *et al.*, 2006).

In general, the vertical directional density function changes depending on the distribution of sources and their relative dominance. When surface noise sources are non-uniform, for instance during a finite-size rain storm, the noise coherence will reflect the location and size of the storm, and rate of the rainfall (Barclay and Buckingham, 2013b). For an individual source, such as a ship, conventional propagation modelling methods can be used to predict the phase interference, or cross-spectral density, across an array. Broadband matched field processing on a VLA has been proven an effective technique for source ranging with many applications (Baggeroer *et al.*, 1988; Brienzo and Hodgkiss, 1993). Although the majority of matched field processing studies rely on coherent processing across large aperture arrays, these modelling techniques are also well suited for predicting the coherence of ship noise on a two-element vertical array. In the case of distantly generated ship noise, which may originate from a number of vessels, the addition of the first few normal modes to the noise field has been shown as an accurate model of the vertical coherence in a shallow water waveguide (Deane *et al.*, 1997). In this article, by treating the pressure time series on a pair of vertical receivers as a linear combination of two processes, wind-driven wave noise and distant or close ship noise, the relative and absolute contributions of each field to the overall soundscape are computed. This is particularly useful in the context of PAM, where metrics include the sound pressure level (SPL) and sound exposure level (SEL) computed over various time intervals and frequency bands (Martin *et al.*, 2019). By first carrying out the source separation described here and then computing these metrics, the contribution of ship noise to SPL and SEL, in the absence of any contribution from the natural background noise, may be uniquely determined and exactly quantified.

The rest of the paper is organized as follows: Sec. II describes measurement details and auxiliary data used for the analysis. Section III shows that the vertical coherence and directionality can be decomposed into a linear combination of terms attributed to uncorrelated source mechanisms, and details the method to determine the relative and absolute contributions of the separate sources to the total field. Vertical noise coherence models of wind-driven ambient noise and ship generated noise are presented in Sec. III. In Sec. IV, the experimental results are described and the implementation of the analysis technique using the coherence models is shown. Section V discusses the application of coherence-based ambient noise data analysis for quantifying the contribution of anthropogenic noise.

II. DATA COLLECTION

The acoustic data used in this analysis were collected on a vertical array deployed near the head of Alvin Canyon south of Martha's Vineyard, Massachusetts, as part of a sound propagation and ambient sound monitoring experiment. The array was deployed from the *R/V Neil Armstrong* on the final leg of the scientific verification cruise from Fairfax, Virginia to its home port, Woods Hole, Massachusetts. The location of the measurement site was at 39° 58.32′ N, 70° 32.94′ W, and is shown in Fig. 1. The water column depth at the mooring location is 350 m. Twenty-nine days of continuous sound pressure time series data were recorded from April 6– May 4, 2016 using Woods Hole Oceanographic Institute's (WHOI) Several Hydrophone Receiving Unit (SHRU) configured as a

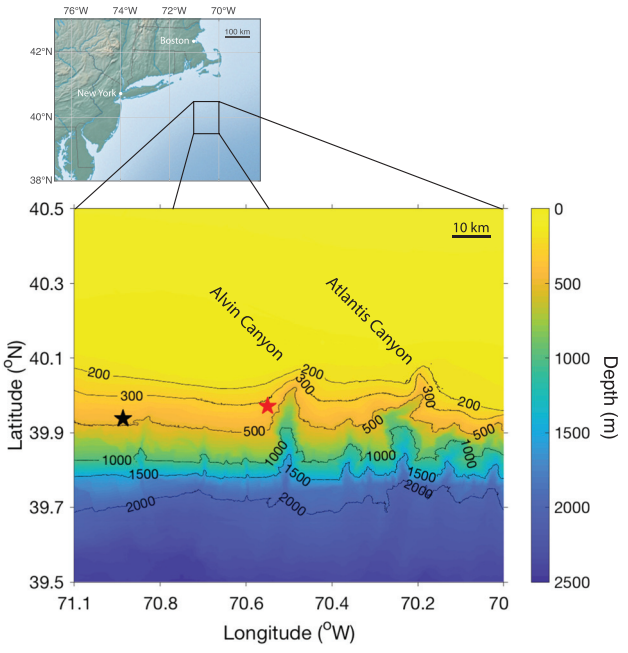

FIG. 1. (Color online) The location of the data collection site (red star) and the Pioneer Array Network mooring (black star) shown along with the bathymetry of the continental shelf break south of Martha's Vineyard, MA.

https://doi.org/10.1121/10.0002922

VLA on a sub-surface mooring. The SHRU VLA consisted of four hydrophones with the top-most sensor (channel 0) positioned at 211.05 m below the surface, and the remaining sensors at depths of 219.03 (channel 1), 219.87 (channel 2), and 220.55 m (channel 3). The hydrophones used in this study were channels 1 and 3, corresponding to an interelement spacing of 1.52 m. All four channels were simultaneously sampled at 9765.625 Hz and subjected to a high-pass filter giving an acoustic bandwidth from 10 to 4880 Hz. The receive sensitivity of the omnidirectional hydrophones was reported by the manufacturer as -170 dB re $1\,V/\mu Pa$.

Temperature and pressure sensors attached along the mooring recorded the water column temperature and mooring tilt, and were sampled every 30 s. Wind speed data were collected from the Central Surface Mooring (CP01CNSM), part of WHOI's coastal observatory network known as the Ocean Observatories Initiative Pioneer Array. The surface mooring, carrying a full meteorology sensor package, provides wind speed adjusted to a height of 10 m above the sea-surface, and is located approximately 30 km from the acoustic receiver at 39° 56.22′ N, 70° 52.62 W(Fig. 1). The data were accessed via the Ocean Observatories Initiative data portal (NSF Ocean Observatories Initiative Data Portal). Geoacoustic seabed properties at the experiment site were determined using U.S. Geological Survey data which reported a compressional sound speed of 1620 m/s (Reid *et al.*, 2005).

III. THEORY

A. Vertical coherence and directional density function

The underwater ambient sound field may be comprised of a linear superposition of two or more noise generating processes provided they are uncorrelated. In the case presented here, wind generated waves breaking at the ocean's surface and noise due to one or more vessels are considered as the primary contributions to the ambient sound field measured on two vertically separated receivers. The acoustic pressure time series at the two vertical separated receivers are given by

$$x_1(t) = w_1(t) + v_1(t) \tag{1}$$

and

$$x_2(t) = w_2(t) + v_2(t), \tag{2}$$

where $w_i(t)$ is due to breaking surface waves and $v_i(t)$ is due to vessels on the i-th hydrophone. The two terms on the right-hand side in each equation are uncorrelated, while both $w_i(t)$ and $v_i(t)$ have some spatial correlation across the two hydrophones. The cross-spectral density between two sensors, S_{ij} is given by

$$\langle S_{ij}(\omega)\rangle = \frac{\langle X_i \cdot X_j^*\rangle}{T}, \tag{3}$$

where X_i is the Fourier transform of x_i, ω is the angular frequency, * denotes the complex conjugate, the angle brackets $\langle\rangle$ indicate an ensemble average, and T is the observation duration. When $i=j$, Eq. (3) describes thePSD. Combining Eqs. (1)–(3) and noting that the ensemble averages of uncorrelated terms go to zero, the cross-spectral density becomes

$$\langle S_{ij}(\omega)\rangle = \frac{\langle W_i \cdot W_j^*\rangle + \langle V_i \cdot V_j^*\rangle}{T}, \tag{4}$$

where W_i and V_i are the Fourier transforms of w_i and v_i respectively, and their dependence on the angular frequency, ω, is implied.

Assuming that both the wave and vessel generated sound fields are spatially homogenous away from the ocean boundaries, and that the receiver separation is small (order several wavelengths) (Buckingham, 1980), the PSD of the total received signal, as well as its components, are independent of receiver position, thus

$$\langle S_{11}\rangle = \langle S_{22}\rangle, \tag{5}$$

$$\langle W_1 \cdot W_1^*\rangle = \langle W_2 \cdot W_2^*\rangle, \tag{6}$$

and

$$\langle V_1 \cdot V_1^*\rangle = \langle V_2 \cdot V_2^*\rangle. \tag{7}$$

The normalized cross-spectral density, or coherence, given by

$$\Gamma_{12}(\omega) = \frac{\langle S_{12}\rangle}{\sqrt{\langle S_{11}\rangle \cdot \langle S_{22}\rangle}}, \tag{8}$$

can then be found by putting Eq. (4) into Eq. (8) and exploiting Eqs. (5)–(7), giving

$$\Gamma_{12}(\omega) = \frac{\langle W_1 \cdot W_2^*\rangle}{\langle W_1 \cdot W_1^*\rangle\langle V_1 \cdot V_1^*\rangle} + \frac{\langle V_1 \cdot V_2^*\rangle}{\langle W_1 \cdot W_1^*\rangle\langle V_1 \cdot V_1^*\rangle}. \tag{9}$$

The denominator in both terms on the right-hand side is the total received power on either sensor, while the numerators are the cross-spectral densities of the wave generated noise in the first term and vessel generated noise in the second.

To further simplify Eq. (9), we define the frequency dependent fraction of total noise power due to vessels as

$$\beta(\omega) = \frac{\langle V_1 \cdot V_1^*\rangle}{\langle S_{11}\rangle}, \tag{10}$$

while the fraction of the noise field due to wave generated sound must then be given by 1- $\beta(\omega)$. With a few algebraic manipulations Eqs. (9) and (10) can be combined to give the vertical noise coherence of the total noise field as

$$\Gamma_{12}(\omega) = (1-\beta)\frac{\langle W_1 \cdot W_2^*\rangle}{\langle W_1 \cdot W_1^*\rangle} + \beta\frac{\langle V_1 \cdot V_2^*\rangle}{\langle V_1 \cdot V_1^*\rangle}, \tag{11}$$

or

$$\Gamma_{12}(\omega) = (1-\beta)\Gamma^{w}_{12}(\omega) + \beta\Gamma^{v}_{12}(\omega). \quad (12)$$

The form shown in Eq. (12) is particularly convenient, as it shows that the second order statistics of the total ambient sound field are a weighted linear combination of the two independent fields. In the case of a normalized statistic, such as the coherence, the weights must sum to unity.

This same property is true for the vertical directional noise density function provided that the noise field may be represented by a summation of plane waves. In this case, the directional noise density is related to the vertical coherence by Cox's equation (Cox, 1973),

$$\Gamma_{12}(\omega) = \frac{1}{2}\int_0^{\pi} F(\theta) e^{i\omega\tau_d \cos\theta} \sin\theta d\theta, \quad (13)$$

under the normalization condition

$$\frac{1}{2}\int_0^{\pi} F(\theta)\sin\theta d\theta = 1, \quad (14)$$

where $F(\theta)$ is the two-dimensional (vertical) directional density function of the total noise field, θ is the polar angle measured from zenith, $i = \sqrt{-1}$, and $\tau_d = d/c$, where d is the spacing between the vertically separated sensors and c is the local sound speed. The directional density function of the total noise field with vertical coherence given by Eq. (12) may be expressed as a weighted sum of the uncorrelated noise fields directionalities (Cox, 1973) using Eq. (13), giving

$$F(\theta) = (1-\beta)F_w(\theta) + \beta F_v(\theta), \quad (15)$$

where $F_w(\theta)$ and $F_v(\theta)$ are the directionalities of the breaking wave-generated and vessel-generated noise fields, respectively. The form of Eqs. (12) and (15) are particularly convenient, as experimentally validated analytical models of wind-wave driven vertical coherence and directionality are available and straightforward to analytically compute in the deep ocean (Cron and Sherman, 1962; Barclay and Buckingham, 2013a) and in a shallow-water Pekeris waveguide (Buckingham, 1980; Kuperman and Ingenito, 1980; Harrison, 1996; Deane *et al.*, 1997), including those with a multi-layered seabed (Carbone *et al.*, 1998; Barclay *et al.*, 2019). In more complex bathymetries, including those where horizontal seabed reflection and refraction are important, computational models may be used to determine the spatial coherence (Barclay and Lin, 2019).

When $\beta = 0$, the noise field coherence and directionality can be determined by the sound generated by surface breaking waves, provided biological, geophysical, or other interfering sources are not present. It should be noted that since the coherence is a normalized quantity, it does not depend on any factor related to the spectral density, such as the effective source level (sea-state and wind speed) or the frequency dependence of the wind-wave generated surface noise, provided there is some acoustic energy in the band of interest. To first order, only the local sound speed, the bathymetry, and the effective (bulk) geoacoustic properties of the seabed must be known. The water column sound speed profile may play a second order effect, apparent in the precise location of the zero-crossings in the real part of the coherence curve (Barclay and Buckingham, 2013a). Wind-generated ambient noise coherence in shallow waters is a stable, time-independent noise property provided sufficient time averaging is used to include contributions from sources covering the entire effective surface listening area of the sensor (Farmer and Vagle, 1988; Deane *et al.*, 1997; Carbone *et al.*, 1998).

When a contribution to the ambient sound field from distant shipping is apparent ($\beta > 0$), the resultant change in coherence can also be seen in the directionality. The component of vessel generated noise which propagates long distances (>10 km) is characterized as low-frequency (<1 kHz) and containing low-order modes (Jensen *et al.*, 1994), and can be modeled accordingly. A careful examination of Cox's equation, Eq. (13), shows that the real part of the coherence is related to the symmetrical component of the noise directionality about the horizontal, while the imaginary part is related only to the asymmetrical component. Since distant vessel noise is best modeled as a summation of low-order modes, $F_v(\theta)$ is predominantly symmetrical about the horizontal, and ship noise will contribute primarily to the real part of the vertical coherence.

From Eqs. (12) and (15), it is clear that to partition the energy in the measured spectral power density between wave generated noise and vessel noise, the coefficient $\beta(\omega)$ must be estimated. In practice, the noise coherence on the left-hand side in Eq. (12) is computed from the measured data while the time-independent wind-generated ambient noise coherence is modelled and held constant over the observation period (Deane *et al.*, 1997; Carbone *et al.*, 1998). $\Gamma^{v}_{12}(\omega)$ can be modelled taking into account the sound propagation environment and the effective range to the ship. Solving for $\beta(\omega)$ then allows the spectral power due to vessel noise to be determined from Eq. (10). The absolute power of received ship noise (RL) in dB re 1 μPa^2/Hz can be found by computing

$$RL(\omega) = 10 * log\{\langle S_{11}(\omega)\rangle \cdot \beta(\omega)\}, \quad (16)$$

while the relative contribution of the VN in dB above the natural background noise can simply be expressed as

$$VN(\omega) = 10 * log\left\{\frac{\beta(\omega)}{1-\beta(\omega)}\right\}. \quad (17)$$

The estimation of the time-dependent parameters RL and VN in long-duration PAM data sets allows the sound exposure of the receiver to vessel generated noise to be quantified and compared against the same metric from the natural ambient soundscape. The theoretical formulas describing the analytical models of wind-wave generated noise and vessel noise used in this study are described in Sec. III B and C.

https://doi.org/10.1121/10.0002922

B. Wind driven ambient noise model

The analytical model of the vertical noise coherence function in an isovelocity fluid layer over an elastic bottom half-space is developed in this section with monopole sources randomly distributed on a plane just below the pressure release surface at depth z_s. Assuming azimuthal symmetry in a cylindrical coordinate system (r,z, φ), the cross spectral density for a single source can be expressed in terms of the depth dependent Green's function

$$S_{12}(\omega) = 2Q^2 G(r, z_s, z_1, \omega) G^*(r, z_s, z_2, \omega), \tag{18}$$

where Q is the source strength, the source depth is z_s, r is the horizontal range between the source and the receiver, and $G(.)$ are Green's functions between the source and each of the receivers at depths z_1 and z_2. Equation (18) can then be integrated for the distribution of sources over all azimuth and range to find the cross-spectral density, giving

$$S_{12}(\omega) = 4\pi v Q^2 \int_0^\infty G(r, z_s, z_1, \omega) G^*(r, z_s, z_2, \omega) r dr, \tag{19}$$

where v is the mean rate of wave breaking events per unit area, and azimuthal symmetry has been assumed. The Green's function solution for the noise field can be expressed as a sum of normal modes (Worzel *et al.*, 1948). For an isovelocity profile, the normal mode decomposition of the Green's functions for a fluid waveguide over a lossy, elastic half-space with a sufficiently slow shear speed can be computed using the complex effective depth approach (Zhang and Tindle, 1993), where the mode functions become trigonometric functions, and the modal eigenvalues can be efficiently and exactly computed (Chapman *et al.*, 1989). The Green's function is then the modal sum

$$G(r, \omega, z_i) = i\pi \sum_{n=1}^{\infty} N_n^2 \sin(\gamma_n z_s) \sin(\gamma_n z_1) H_0^1(k_n r), \tag{20}$$

where γ_n is the vertical wavenumber, n is the mode number, and $H_0^1(.)$ is the zeroth order Hankel function of the first kind which depends on the modal eigenvalue k_n and the range. The mode amplitude, N_n, which depends on seabed reflection loss and a practical upper limit to the sum in Eq. (20) for long distance propagating modes, can be obtained by following the complex effective depth approach (Zhang and Tindle, 1993). By substituting the modal expansion of the Green's functions into Eq. (18) and exploiting the orthogonality of the Hankel functions to compute the integral over range, the cross-spectral density for the entire surface area can be simplified to the double modal sum:

$$S_{12}(\omega) = 16\pi v Q^2 \sum_{n=1}^{\infty} N_n^2 \sin(\gamma_n z_s) \sin(\gamma_n z_1) \times \sum_{m=1}^{\infty} N_m^{*2} \sin(\gamma_m z_s) \sin(\gamma_m z_2) \frac{\ln(k_n / k_m^*) - i\pi}{k_m^{*2} - k_n^2}, \tag{21}$$

where n indexes over the first Green's function, and m the second. The cross-spectral density reduces to the PSD when $z_1 = z_2$, so Eq. (21) can be combined with Eq. (8) to give the vertical noise coherence in a shallow water, isovelocity waveguide with an elastic seabed.

C. Ship noise model

To model shipping, the pressure field generated by a single source is computed using the same normal mode solution for a shallow water waveguide. The Green's function to describe the acoustic pressure due to a single source in the wave guide is given by Eq. (20), where z_s is now the source depth of the vessel. The power spectrum and cross-spectrum can be computed by directly substituting Eq. (20) into Eq. (18), providing all the necessary terms for the vertical coherence shown in Eq. (8). In this case, the received sound level, coherence, and directionality depend on the range between the receiver and vessel. Thus, the resultant coherence due to ship noise can be expressed as a function of range and frequency.

IV. DATA AND RESULTS

A. Acoustic data analysis

Time-series ambient noise data from the top-most hydrophone (channel 0) in SHRU were used to calculate the PSD. A total of 120 estimates of the PSD were made every minute using a 9765-point fast Fourier transform, corresponding to an interval time of 1 s, each with a 50% overlap and tapered with a Hann window. These estimates were averaged every 60 s to produce a single PSD for each one-minute recording, and a long-term spectrogram was produced by concatenating the results over the entire period of observation (Fig. 2)(a). At low frequencies (below 500 Hz), non-radiating pressure fluctuations caused by flow over the surface of hydrophone, as well as mooring motion dominate the PSD. The daily modulation in the PSD in this band occurs with the frequencies of the local tidal cycles.

The sound generated by ship traffic is present in this frequency band and extends up to 1.5 kHz when vessels are present. Although the presence of vessels can be identified in the spectrogram, quantifying their contribution to the total ambient sound field using the PSD with dynamic environment conditions is cumbersome. When there is no vessel near (<10 km) the receiver, the band 0.5–4.8 kHz is dominated by sea-surface agitation related to wind generated waves. The qualitative relationship between sea-state and sound level in the frequency band 1.95–2.05 kHz is shown in Fig. 2(b) where the five-minute averaged wind speed is plotted along with the PSD.

The cross-spectrum was calculated using the same parameters as the PSD and normalized by the respective PSD from each sensor to retrieve the vertical noise coherence as described by Eq. (8). The real and imaginary parts of the coherence over the entire data collection period are shown as a coherogram (analogous to a spectrogram) in

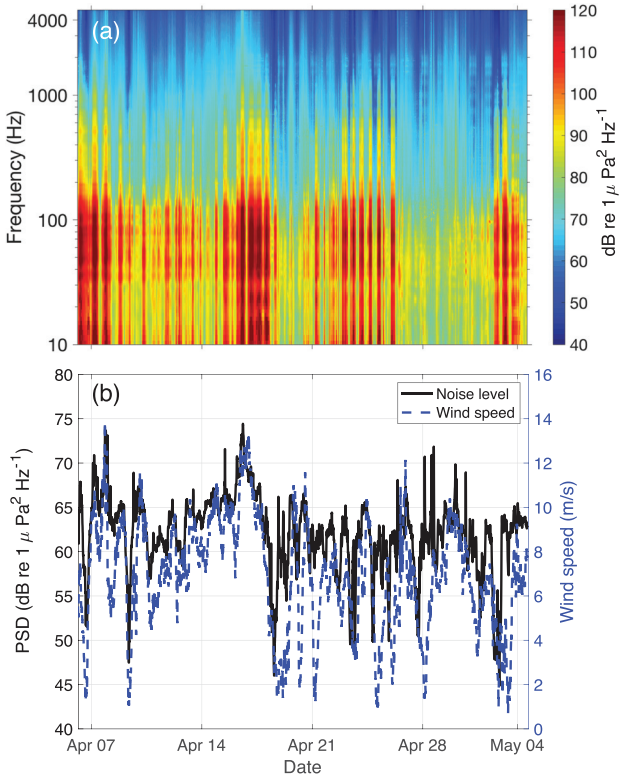

FIG. 2. (Color online) (a) Spectrogram of the entire period of observation from the top hydrophone (channel 0), and (b) the comparison between the five-minute averaged wind speed and the PSD in the frequency band 1.95–2.05 kHz.

Fig. 3. Degradation in the coherence at low frequencies (below 500 Hz, or 3.2 in dimensionless frequency) is visible in both real and imaginary components of the coherogram caused by non-radiated (spatially uncorrelated) pressure fluctuations, or flow noise, on the individual sensors. The oscillatory nature of wind-generated ambient noise coherence is evident in the coherogram (above 500 Hz, or 3.2 in dimensionless frequency), with stable zero crossings in frequency for the entire period of observation. The coherogram shows deviation from normal wind-coherence at certain

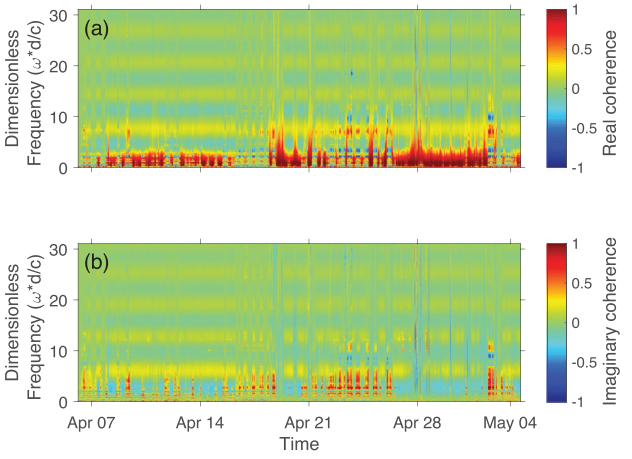

FIG. 3. (Color online) The (a) real and (b) imaginary components of the coherence as a function of frequency for the entire period of observation.

periods due to local and distant ship traffic. Close inspection of the vertical noise coherence reveals the presence of distant shipping in the dataset below 1.5 kHz, or 9.5 in dimensionless frequency, which can be identified as a broadband increase in real coherence, while several close-range ships can be identified by short-duration spikes over the entire acoustic bandwidth in both the real and imaginary components.

Each one-minute sample that makes up the coherogram can be categorized into three main source classes: wind-generated, close-range ship, and distant shipping. Examples of the real and imaginary coherence components of these distinct sources are shown in Fig. 4. The most dominant and stable coherence pattern observed in the dataset is caused by wind generated ambient noise alone, showing oscillating curves with several zero crossings, with decreasing coherence and increasing dimensionless frequency. The presence of the imaginary component indicates an asymmetry in the noise field, while the amplitude suggests energy is propagating downward with weaker reflection from the seabed.

The second class of coherence present in the data is that of an individual close range (< 10 km) ship, where the wind-generated noise is masked. The real and imaginary components show a high coherence over the entire frequency range with several zero crossings that depend on the distance between the source and the receivers. As the ship passes by the receiver, a bathtub shaped phase interference pattern is formed in the coherogram due to the interaction between direct waves and their reflection from the waveguide boundaries.

The third class of coherence observed is due to distant shipping in the frequency band 0.1–1.5 kHz. At frequencies above 1.5 kHz, the coherence follows that of the wind-generated curve, since the typical vessel source spectrum, which decreases in power with increasing frequency, and the attenuation of propagating sound, caused by bottom interaction, increase with frequency and fall below the background noise. At frequencies below 1.5 kHz, low order modes (near horizontally propagating sound) arrive at the sensors very nearly in phase and raise the real part of the coherence, while pushing the imaginary component towards zero due to the increased symmetry in the noise field. The alteration in the coherence pattern due to distant shipping depends on both the range and relative power of the ship noise level compared to the background wind-generated noise.

The three classes of coherence shown in Fig. 4 were simulated using analytical models described in Sec. III. The modelled vertical coherence of ambient noise computed using Eq. (21) is compared with data in Figs. 4(a) and 4(b). The water column sound speed ($c_w = 1494\,m/s$) and density ($\rho_w = 1024\,kg/m^3$) were obtained from conductivity, temperature, and depth (CTD) data at the receiver position. The compressional sound speed of sediment was taken from U.S. Geological Survey data ($c_c = 1620\,m/s$) close to the noise measurement location. For the remaining geoacoustic properties, such as shear speed ($c_s = 45\,m/s$), density ($\rho_b = 1900\,kg/m^3$), compressional

https://doi.org/10.1121/10.0002922

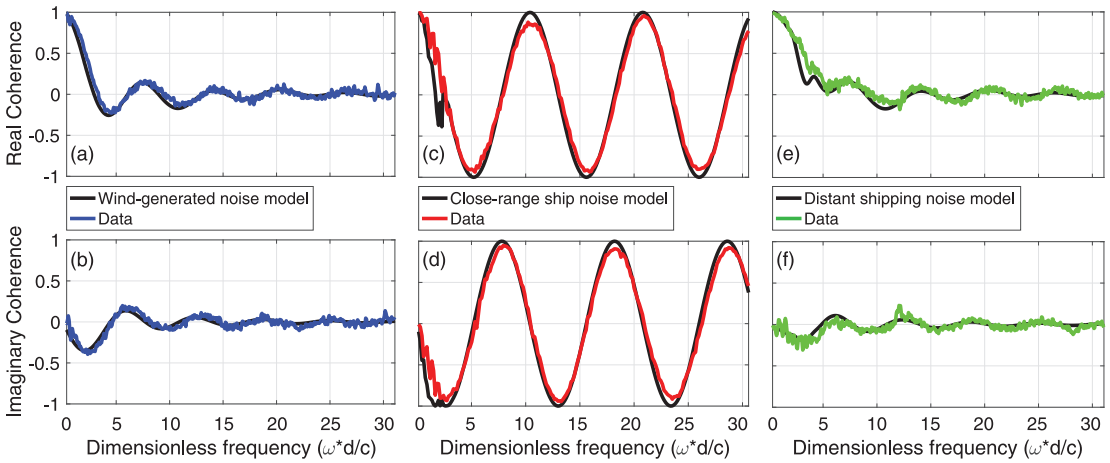

FIG. 4. (Color online) The real and imaginary components of the three classes of observed coherence: (a)–(b) wind generated data (blue) and model (black), (c)–(d) individual close-range ship data (red) and model (black), and (e)–(f) distant shipping data (green) and model (black).

attenuation $(\alpha_c = 0.9\,dB/\lambda)$, and shear attenuation $(\alpha_s = 2\,dB/\lambda)$, Hamilton's geoacoustic model for the continental slope environment was used (Baggeroer *et al.*, 1988; Brienzo and Hodgkiss, 1993).

The coherence for noise from an individual ship at close range was computed by substituting Eq. (20) with the source depth as 7 m (z_s) into Eq. (19), using the same geoacoustic parameters listed above, and by brute force searching over the unknown horizontal range parameter (Wales and Heitmeyer, 2002; Gassmann *et al.*, 2017). The best fit between model output and data occurred at 380 m, which is the closest point of approach for this particular contact, shown in Figs. 4(c) and 4(d). The figure shows the comparison of real and imaginary coherence between data and model. Model data comparisons of vertical coherence are an effective method for ranging ships in shallow water waveguides (Shajahan and Barclay, 2019).

The vertical coherence of distant shipping was simulated using both the ambient noise model given by Eqs. (21) and (8), and the normal mode sound propagation model given by combining Eqs. (18), (20), and (8). Note that the details of the source spectrum (e.g., the wave breaking rate per unit area, ν), cancel in Eq. (8). The cross-spectral density (CSD) and PSD were also calculated by the incoherent sum of the first 10 modes computed using Eq. (20), where the ship was assumed to be stationary at a distance of 10 km. The comparison between data and model with the same geoacoustic parameters as described above is shown in Figs. 4(e) and 4(f), where the best-fit relative power between the distant ship noise and wind-generated noise was determined by brute force search over $\beta(\omega)$.

B. Quantifying ship noise

To determine the relative contribution of ship noise to the total power spectrum, $\beta(\omega)$ must be estimated by inverting Eq. (12). A combination of the wind driven ambient noise and ship noise models derived from Eqs. (18)–(21) can be used to compute $\Gamma_{12}^{w}(\omega)$ and $\Gamma_{12}^{v}(\omega)$, where the latter depends on the range between the ship and receiver. In general, the frequency dependence of $\beta(\omega)$ should reflect frequency dependence of a typical vessel. A closed-form model adapted from Deane *et al.* (1997) gives the frequency dependence for $\beta(\omega)$,

$$\beta(\omega) = \frac{2\tilde{\beta}}{(\omega/\omega_1)^n + (\omega_1/\omega)^n}, \tag{22}$$

where n determines the roll-off in dB per octave and ω_1 is the peak frequency of the source, chosen to be 350 Hz. The inversion in Eq. (12) now depends on three free parameters: range $(R = 0.1 - 15\,km)$, roll-off $(n = 2 - 6\,dB/octave)$, representing a broad description of the ship's source spectrum, and relative weighting $(\tilde{\beta} = 0 - 1)$, where the values in the parentheses are the search domains for each variable. The inversion method is a brute force search over the three parameters aiming to minimize the error between simulated coherence [the right-hand side of Eq. (12)] and measured coherence [the left-hand side of Eq. (12)] at each time step. The inversion was carried out at each 5-min interval of acoustic data over the entire period of observation. The best-fit between model and data was determined by minimizing the value of root mean square (RMS) error computed as

$$\xi(R,\beta,n) = \frac{1}{N}\sqrt{\sum_{i=1}^{N}\left[\Gamma_{12}^{data}(\omega_i) - \Gamma_{12}^{model}(\omega_i,R,\beta,n)\right]^2}, \tag{23}$$

where N is the total number of frequency points in the band 350 Hz–4.8 kHz, and Γ_{12}^{model} and Γ_{12}^{data} are the simulated and measured coherence, respectively. The band-limited computation of the RMS error was chosen to avoid misfit caused by flow noise and motivated the choice of the peak source frequency, although large sea-going vessels typically have a source spectrum with a peak below this low-frequency limit. The absolute coherogram of the measurement, the corresponding best fit after inversion, and the fit residual are shown in in Figs. 5(a)–5(c), respectively.

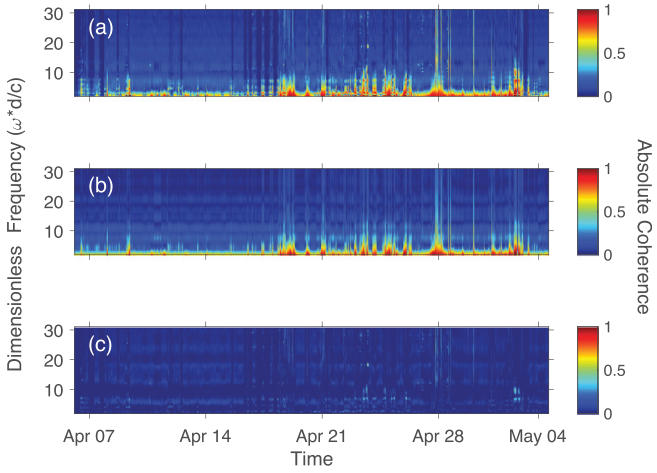

FIG. 5. (Color online) The (a) measured and (b) best-fit modeled absolute vertical noise coherence over the observations period, and (c) the fit residuals.

The time series of the coherogram from the inversion results compared very well with the measured coherogram. The two-component noise coherence model given by Eq. (12) distinctly reproduces the observed effects of both distant and close-range shipping. Some features of the data not reproduced by the model may be due to biological sources in the vicinity of the receivers, or by strong tones present in the ship noise spectra which cannot be captured by the model presented in Eq. (22).

The estimated relative contribution of ship noise to the total sound field is shown in terms of the fraction of total power, or $\beta(\omega)$, in Fig. 6(a) and in terms of relative power

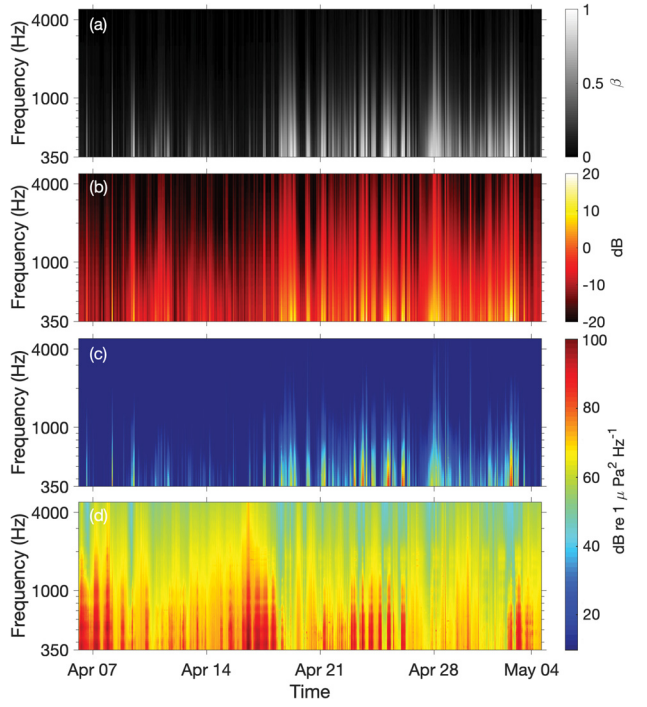

FIG. 6. (Color online) The (a) best-fit of $\beta(\omega)$ after inversion, (b) relative contribution of shipping to the overall noise field, (c) absolute contribution of shipping to the overall noise field, and (d) total received noise level.

measured in dB in Fig. 6(b). During the first half of observation, the influence of shipping is limited to distant passing ships, while in the second half, distant and close-range shipping is present, shown by the high values of $\beta(\omega)$ across the entire band. During the second half of the recording, ship noise dominates the soundscape below 1 kHz with $\beta \sim 1$. When individual ships approach the receiver, the relative ship noise contribution is as much as 40 dB above the wind generated background sound at low frequencies, which is consistent with previously reported studies (Wales and Heitmeyer, 2002). The received level solely due to ship noise can be estimated from the inversion result of $\beta(\omega)$ and total received noise by Eq. (16). The power of RL at the sensor in dB re 1 μPa^2/Hz and total noise power are shown in Figs. 6(c) and 6(d), respectively.

In order to demonstrate the effectiveness of this method in partitioning the total noise field into shipping and wind noise components, the correlation coefficients between the noise power and wind speed at 10 m above the sea surface, shown in Fig. 2, were computed and compared using either the total received noise or the inversion-derived wind-generated noise. The coefficient of determination (r^2) between a five-minute averaged total received noise level and wind speed at 500 Hz, and 1, 2, and 3 kHz was computed and shown along with the data in Fig. 7(a)–7(d). At 0.5 kHz the noise level shows a very weak correlation ($r^2 = 0.07$) with wind speed due to the masking by ship noise. As the frequency increases from 0.5 to 3 kHz, r^2 also improves from a low to moderate positive correlation due to the frequency dependent nature of ship noise.

The inverted noise contribution due to shipping was subtracted from the total received level to produce an estimate of the purely wind-generated noise field, which was then plotted against wind speed and used to compute the r^2 values, shown in Figs. 7(e)–7(h). At the lowest frequency (500 Hz), a greater than fivefold increase in the value of correlation coefficient ($r^2 = 0.37$) is seen. As the frequency increases, the ship noise contribution diminishes and the improvements in r^2 decrease to 8% at 3 kHz. This demonstrates the effectiveness of noise field separation by considering the vertical coherence as a linear combination of wind and ship noise in quantifying the impact of anthropogenic activity on the marine habitat.

V. CONCLUSIONS

A processing technique for time-series ambient noise data based on spatial coherence has been described in this paper. The coherogram can be used for classifying the time variance of major noise sources present in the environment. The analysis involves the use of data in association with noise models to understand the impact of different sources on noise spatial characteristics. The surface distributed noise as well as distant and close-range shipping were identified as the major sources of sound present in the measurement. Analytical models of ambient noise and sound propagation were used to simulate vertical coherence for

https://doi.org/10.1121/10.0002922

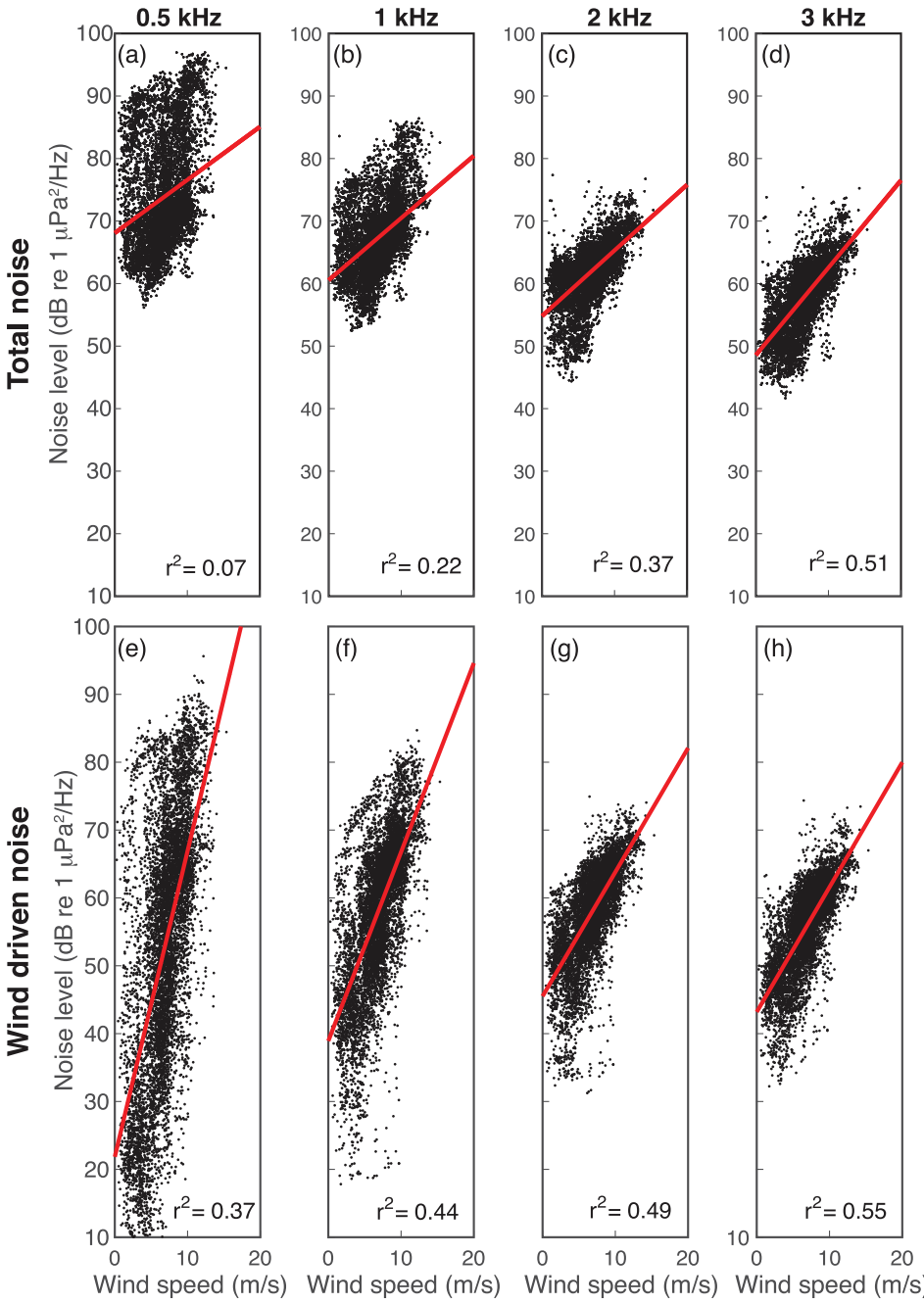

FIG. 7. (Color online) Correlation coefficient analysis between wind speed and (a)–(d) total received noise level, and (e)–(h) best-fit wind-generated noise level at 500 Hz, and 1, 2, and 3 kHz.

comparison with experimental data. The data-model fitting of the coherence was able to provide both the relative and absolute contribution of ship noise to the overall sound field, along with an estimate of source position, as a function of time.

In recent years, the ambient noise level in the ocean has increased due to a growth of commercial ship traffic. Continuous long-term monitoring is required to understand the effect of anthropogenic noise on marine species. The present work confirms the advantage of using a pair of vertically aligned hydrophones in long-term PAM systems for a quantitative estimate of the anthropogenic contribution to the soundscape. The coherence-based analysis presented here is able to quantify the impact of ship noise as a function of time and frequency, without the need for additional data such as wind speed and ship distribution.

ACKNOWLEDGMENTS

The authors would like to thank the Captain and crew of the *R/V Neil Armstrong* for assistance with the collection of data. The work was funded by Office of Naval Research, Code 32 (Grant No. N00014-17-1-2692 for Y.T. Lin), and the Canada Research Chair program and the Natural Science and Engineering Research Council Discovery program. N. S. would like to thank Transatlantic Ocean System Science and Technology (TOSST) for his graduate fellowship.

Aulanier, F., Simard, Y., Roy, N., Gervaise, C., and Bandet, M. (**2017**). "Effects of shipping on marine acoustic habitats in Canadian Arctic estimated via probabilistic modeling and mapping," Mar. Pollut. Bull. **125**, 115–131.

Baggeroer, A. B., Kuperman, W., and Schmidt, H. (**1988**). "Matched field processing: Source localization in correlated noise as an optimum parameter estimation problem," J. Acoust. Soc. Am. **83**, 571–587.

Barclay, D. R., Bevans, D. A., and Buckingham, M. J. (**2019**). "Estimation of the geoacoustic properties of the New England Mud Patch from the vertical coherence of the ambient noise in the water column," IEEE J. Oceanic Eng. **45**, 51–59.

Barclay, D. R., and Buckingham, M. J. (**2013a**). "Depth dependence of wind-driven, broadband ambient noise in the Philippine Sea," J. Acoust. Soc. Am. **133**, 62–71.

Barclay, D. R., and Buckingham, M. J. (**2013b**). "The depth-dependence of rain noise in the Philippine Sea," J. Acoust. Soc. Am. **133**, 2576–2585.

Barclay, D. R., and Lin, Y.-T. (**2019**). "Three-dimensional noise modeling in a submarine canyon," J. Acoust. Soc. Am. **146**, 1956–1967.

Brienzo, R. K., and Hodgkiss, W. S. (**1993**). "Broadband matched-field processing," J. Acoust. Soc. Am. **94**, 2821–-2831.

Buckingham, M. J. (**1980**). "A theoretical model of ambient noise in a low-loss, shallow water channel," J. Acoust. Soc. Am. **67**, 1186–1192.

Buckingham, M. J. (**2013**). "Theory of the directionality and spatial coherence of wind-driven ambient noise in a deep ocean with attenuation," J. Acoust. Soc. Am. **134**, 950–958.

Buckingham, M. J., and Jones, S. A. (**1987**). "A new shallow-ocean technique for determining the critical angle of the seabed from the vertical directionality of the ambient noise in the water column," J. Acoust. Soc. Am. **81**, 938–946.

Carbone, N. M., Deane, G. B., and Buckingham, M. J. (**1998**). "Estimating the compressional and shear wave speeds of a shallow water seabed from the vertical coherence of ambient noise in the water column," J. Acoust. Soc. Am. **103**, 801–813.

Chapman, D. M., Ward, P. D., and Ellis, D. D. (**1989**). "The effective depth of a Pekeris ocean waveguide, including shear wave effects," J. Acoust. Soc. Am. **85**, 648–653.

Chapman, N. R., and Price, A. (**2011**). "Low frequency deep ocean ambient noise trend in the Northeast Pacific Ocean," J. Acoust. Soc. Am. **129**, EL161–EL165.

Cox, H. (**1973**). "Spatial correlation in arbitrary noise fields with application to ambient sea noise," J. Acoust. Soc. Am. **54**, 1289–1301.

Cron, B. F., and Sherman, C. H. (**1962**). "Spatial-correlation functions for various noise models," J. Acoust. Soc. Am. **34**, 1732–1736.

Deane, G. B., Buckingham, M. J., and Tindle, C. T. (**1997**). "Vertical coherence of ambient noise in shallow water overlying a fluid seabed," J. Acoust. Soc. Am. **102**, 3413–3424.

Erbe, C., MacGillivray, A., and Williams, R. (**2012**). "Mapping cumulative noise from shipping to inform marine spatial planning," J. Acoust. Soc. Am. **132**, EL423–EL428.

Farmer, D. M., and Vagle, S. (**1988**). "On the determination of breaking surface wave distributions using ambient sound," J. Geophys. Res. **93**, 3591–3600, https://doi.org/10.1029/JC093iC04p03591.

Frisk, G. V. (**2012**). "Noiseonomics: The relationship between ambient noise levels in the sea and global economic trends," Sci. Rep. **2**, 1–4.

Gassmann, M., Wiggins, S. M., and Hildebrand, J. A. (**2017**). "Deep-water measurements of container ship radiated noise signatures and directionality," J. Acoust. Soc. Am. **142**, 1563–1574.

Gervaise, C., Aulanier, F., Simard, Y., and Roy, N. (**2015**). "Mapping probability of shipping sound exposure level," J. Acoust. Soc. Am. **137**, EL429–EL435.

Harris, P., Sotirakopoulos, K., Robinson, S., Wang, L., and Livina, V. (**2019**). "A statistical method for the evaluation of long term trends in underwater noise measurements," J. Acoust. Soc. Am. **145**, 228–242.

Harrison, C. H. (**1996**). "Formulas for ambient noise level and coherence," J. Acoust. Soc. Am. **99**, 2055–2066.

Ingenito, F., and Wolf, S. N. (**1989**). "Site dependence of wind-dominated ambient noise in shallow water," J. Acoust. Soc. Am. **85**, 141–145.

Jensen, F. B., Kuperman, W. A., Porter, M. B., and Schmidt, H., *Computational Ocean Acoustics* (Springer-Verlag, New York, NY, **1994**).

Kuperman, W. A., and Ingenito, F. (**1980**). "Spatial correlation of surface generated noise in a stratified ocean," J. Acoust. Soc. Am. **67**, 1988–1996.

Martin, S. B., Morris, C., Bröker, K., and O'Neill, C. (**2019**). "Sound exposure level as a metric for analyzing and managing underwater soundscapes," J. Acoust. Soc. Am. **146**, 135–149.

McDonald, M. A., Hildebrand, J. A., and Wiggins, S. M. (**2006**). "Increases in deep ocean ambient noise in the Northeast Pacific west of San Nicolas Island, California," J. Acoust. Soc. Am. **120**, 711–718.

Merchant, N. D., Witt, M. J., Blondel, P., Godley, B. J., and Smith, G. H. (**2012**). "Assessing sound exposure from shipping in coastal waters using a single hydrophone and Automatic Identification System (AIS) data," Mar. Pol. Bull. **64**, 1320–1329.

Miksis-Olds, J. L., and Nichols, S. M. (**2016**). "Is low frequency ocean sound increasing globally?," J. Acoust. Soc. Am. **139**, 501–511.

Muzi, L., Siderius, M., and Gebbie, J. (**2018**). "An analysis of beamforming algorithms for passive bottom reflection-loss estimation," J. Acoust. Soc. Am. **144**, 3046–3054.

Muzi, L., Siderius, M., and Nielsen, P. L. (**2016**). "Frequency based noise coherence-function extension and application to passive bottom-loss estimation," J. Acoust. Soc. Am. **140**, 1513–1524.

Muzi, L., Siderius, M., Quijano, J. E., and Dosso, S. E. (**2015**). "High-resolution bottom-loss estimation using the ambient-noise vertical coherence function," J. Acoust. Soc. Am. **137**, 481–491.

NSF Ocean Observatories Initiative Data Portal. "Mean wind speed (CP04 OSSM-SBD11-06-METBKA000) data from 05 April 2016 to 05 May 2016," https://oceanobservatories.org (Last viewed 15 March 2017).

Nystuen, J. A., McGlothin, C. C., and Cook, M. S. (**1993**). "The underwater sound generated by heavy rainfall," J. Acoust. Soc. Am. **93**, 3169–3177.

Popper, A. N., and Hawkins, A., *The Effects of Noise on Aquatic Life II* (Springer, New York, NY, **2016**).

Putland, R. L., Merchant, N. D., Farcas, A., and Radford, C. A. (**2018**). "Vessel noise cuts down communication space for vocalizing fish and marine mammals," Glob. Change Biol. **24**, 1708–1721.

Reid, J. M., Reid, J. A., Jenkins, C. J., Hastings, M. E., Williams, S. J., and Poppe, L. J. (**2005**). "usSEABED: Atlantic coast offshore surficial sediment data release," U.S. Geological Survey Data Series 118, version 1.0, https://pubs.usgs.gov/ds/2005/118/ (Last viewed April 27, 2020).

Rolland, R. M., Parks, S. E., Hunt, K. E., Castellote, M., Corkeron, P. J., Nowacek, D. P., Wasser, S. K., and Kraus, S. D. (**2012**). "Evidence that ship noise increases stress in right whales," Proc. Roy. Soc. B: Biol. Sci. **279**, 2363–2368.

Shajahan, N., and Barclay, D. R. (**2019**). "The effect of submarine canyon bathymetry on range estimation using cross-correlated ship noise field," J. Acoust. Soc. Am. **146**, 2858–2858.

Siderius, M., Harrison, C. H., and Porter, M. B. (**2006**). "A passive fathometer technique for imaging seabed layering using ambient noise," J. Acoust. Soc. Am. **120**, 1315–1323.

Siderius, M., Muzi, L., Harrison, C. H., and Nielsen, P. L. (**2013**). "Synthetic array processing of ocean ambient noise for higher resolution seabed bottom loss estimation," J. Acoust. Soc. Am. **133**, EL149–EL155.

Vagle, S., Large, W. G., and Farmer, D. M. (**1990**). "An evaluation of the WOTAN technique of inferring oceanic winds from underwater ambient sound," J. Atmos. Ocean. Technol. **7**, 576–595.

Wales, S. C., and Heitmeyer, R. M. (**2002**). "An ensemble source spectra model for merchant ship-radiated noise," J. Acoust. Soc. Am. **111**, 1211–1231.

Wenz, G. M. (**1962**). "Acoustic ambient noise in the ocean: Spectra and sources," J. Acoust. Soc. Am. **34**, 1936–1956.

Worzel, J. L., Pekeris, C. L., and Ewing, W. M., *Propagation of Sound in the Ocean: Explosion Sounds in Shallow Water* (Geological Society of America, Boulder, CO, **1948**).

Zhang, Z., and Tindle, C. (**1993**). "Complex effective depth of the ocean bottom," J. Acoust. Soc. Am. **93**, 205–213.